Density Functional Study of C−H and O−H Bond Activation by Transition Metal d^0−Oxo Complexes: 1. Thermodynamic Considerations

Liqun Deng and Tom Ziegler*

Department of Chemistry, University of Calgary, Calgary, Alberta, Canada T2N 1N4

Received January 16, 1996[⊗]

Density functional methods have been applied to the thermochemistry of methanol C−H and O−H bond activation by group 5 through group 8 transition metal (TM)−oxo model complexes. Two channels have been investigated for both the C−H and O−H bond cleavage: i.e., abstraction of the hydrogen by the TM−oxo complexes and addition of the C−H or O−H bond to the M═O linkage. Structures of all species involved in these processes were fully optimized and further confirmed to be energy minimum points on the potential energy surfaces by frequency calculations. It is shown that the reaction enthalpies for all TM systems under investigation follows the order O−H hydrogen abstraction > C−H hydrogen abstraction > C−H bond addition > O−H bond addition. The O−H addition process was found for most of the systems to be a thermodynamically feasible channel. On the other hand, abstraction of a hydrogen from the O−H bond is for all but the Fe systems too endothermic to proceed. For the hydrogen abstraction channel, endothermicity of the reactions increases down a given TM triad and decreases from left to right within a transition series. The opposite trend was found for the C−H or O−H bond addition processes. A detailed analysis of the theoretical MO−H, M-OCH_3, and M-CH_2OH bond energies revealed that the energy gap between the HOMO and LUMO of the TM d^0−oxo complexes is responsible for the periodic trends in the calculated reaction enthalpies. Our thermochemical estimates were further used to explain why the preferred pathway for O−H and C−H activation by TM oxo complexes changes with the position of the metal in the periodic table.

1. Introduction

The activation of C−H or O−H bonds is an essential step in many important chemical and biological processes.[1] High-valent transition metal (TM)−oxo complexes have long been recognized to facilitate reactions of this type.[2] For example, cytochrome P-45 enzymes mitigate a wide range of biochemical oxidation processes in which a reactive intermediate with an Fe−O bond is involved.[2d,3] Further, some ruthenium−oxo complexes have been successfully designed to catalytically oxidize a variety of organic substrates.[4] Other oxo species with formal d^0 to d^2 transition metal centers such as pentavalent vanadium,[2e] chromyl chloride,[2e,5] molybdenum(VI) complexes,[6] permanganate,[1f,7] ferrate,[8] ruthenate,[9] ruthenium tetraoxide,[10] and osmium tetraoxide[11] have all proven to be effective reagents for oxidizing specific alkanes and alcohols. The widespread practical use of oxometal complexes in C−H and O−H bond cleavage has spurred considerable interest into the underlying activation mechanism, with kinetic studies dating back to the early 1960s.[1−10]

It seems to be the general consensus that C−H or O−H bond activation by oxometal compounds may proceed through two different channels: (i) transfer of a hydrogen or hydride from the C−H or O−H bond to a terminal oxygen of the oxometal compound; (ii) addition of a C−H or O−H bond to the M═O linkage to form a transition metal complex. However, experimental input

[⊗] Abstract published in *Advance ACS Abstracts,* June 1, 1996.

(1) (a) *Selective Hydrocarbon Activation, Principles and Progress*; Davies, J. A., Watson, P. L., Liebman, J. F., Greenberg, A., Eds.; VCH: New York, 1990. (b) *Activation and Functionalization of Alkanes*; Hill, C. L., Ed.; Wiley: New York, 1989. (c) *Oxidation in Organic Chemistry*; Wiberg, K. B., Ed.; Academic Press: New York, 1965; Part A. (d) Stewart, R. *Oxidation Mechanisms*; Benjamin: New York, 1964.

(2) (a) Parshall, G. W.; Ittel, S. D. *Homogeneous Catalysis,* 2nd ed.; Wiley-Interscience: New York, 1992. (b) Nugent, W. A.; Mayer, J. M. *Metal-Ligand Multiple Bonds*; Wiley: New York, 1988. (c) Holm, R. H. *Chem. Rev.* **1987**, *87*, 1401. (d) *Cytochrome P-450: Structure, Mechanism, and Biochemistry*; Ortiz de Montellano, P. R., Ed.; Plenum: New York, 1986. (e) *Organic Syntheses by Oxidation with Metal Compounds*; Mijs, W. J., de Jonge, C. R. H. I., Eds.; Plenum: New York, 1986. (f) Shilov, A. E. *Activation of Saturated Hydrocarbons by Transition Metal Complexes*; D. Reidel: Dordrecht, The Netherlands, 1984. (g) Sheldon, R. A.; Kochi, J. K. *Metal-Catalyzed Oxidation of Organic Compounds*; Academic Press: New York, 1981.

(3) Groves, J. T.; Nemo, T. E.; Myers, R. S. *J. Am. Chem. Soc.* **1979**, *101*, 1032.

(4) (a) Moyer, B. A.; Thompson, M. S.; Meyer, T. J. *J. Am. Chem. Soc.* **1980**, *102*, 2310. (b) Groves, J. T.; Quinn, R. *J. Am. Chem. Soc.* **1985**, *107*, 5790.

(5) (a) Cook, G. K.; Mayer, J. M. *J. Am. Chem. Soc.* **1995**, *117*, 7139, and references therein. (b) Cook, G. K.; Mayer, J. M. *J. Am. Chem. Soc.* **1994**, *116*, 1855. (c) Sharpless, K. B.; Akashi, K. *J. Am. Chem. Soc.* **1975**, *97*, 5927. (d) Wiberg, K. B. In ref 1d. (e) Mosher, W. A.; Celeste, J. R. *Rev. Chim. Acad. Repub. Pop. Roum.* **1962**, *7*, 1085. (f) Hartford, W. H.; Darrin, M. *Chem. Rev.* **1958**, *58*, 1.

(6) Ishii, Y.; Yamawaiki, K.; Yoshida, T.; Ura, T.; Ogawa, M. *J. Org. Chem.* **1987**, *52*, 1868.

(7) (a) Lee, G. L.; Chen, T. *J. Am. Chem. Soc.* **1993**, *115*, 11231 (b) Lee, G. L.; Chen, T. *J. Org. Chem.* **1991**, *56*, 5341 and references therein.

(8) (a) Lee, D. G.; Cai, H. *Can. J. Chem.* **1993**, *71*, 1394. (b) Tsuda, Y.; Nakajima, S. *Chem. Lett.* **1987**, 1397. (c) Riley, J. T. *Inorg. Chim. Acta* **1974**, *8*, 177. (d) Audette, R. J.; Quail, J. W.; Smith, P. J. *J. Chem. Soc., Chem. Commun.* **1973**, 38.

(9) (a) Lee, D. G.; Congson, L. N. C. *Can. J. Chem.* **1990**, *68*, 1774. (b) Coats, R. M.; Senter, P. D.; Baker, W. R. *J. Org. Chem.* **1982**, *47*, 3597. (c) Gopelan, B.; Larsen, S. D.; Siret, P.; Cras, J. L. *J. Am. Chem. Soc.* **1978**, *100*, 8034.

(10) (a) Lee, D. G. In *Oxidation in Organic Chemistry*; Trahanovsky, W. S., Ed., Academic Press: New York, 1973; Part B. (b) Lee, D. G.; Van den Engh, M. *Can. J. Chem.* **1972**, *50*, 3129.

(11) (a) Singh, H. K. In ref 2d.

S0276-7333(96)00020-9 CCC: $12.00

is usually not sufficient[6b] to rule out either of the mechanistic channels for a reaction involving a specific metal oxide. Chief among the data lacking is reliable information on MO−H, M−alkoxy, and M−hydroxyalkyl bond energies involving high-valent transition metal centers, M. It is not easy to obtain the needed data experimentally, since many of the relevant species in the required thermochemical study are unstable or difficult to isolate. Under these circumstances, a theoretical approach becomes an attractive alternative. However, to date computational studies have been limited to a few investigations based on either *ab initio* methods,[12,13] or density functional theory (DFT).[14]

The most notable earlier theoretical work is that of Rappé and Goddard[15] (RG). The authors applied the generalized valence bond (GVB) method to alkane, alcohol and alkene oxidation by chromyl and molybdenyl chloride. In their pioneering studies, RG have carried out an extensive thermodynamic analysis of the C−H and O−H bond activation processes. Unfortunately, due to limitations in methodology and computational facilities at the time, RG were not able to fully optimize the geometrical structures of the different species involved. Ziegler and Li[14] have more recently carried out a specific DFT study on the C−H and O−H activation in methanol by chromyl chloride (CrO_2Cl_2). Their results indicate that C−H bond activation takes place via the hydrogen abstraction channel, whereas the O−H bond cleavage proceeds via an addition of the O−H bond to the M=O linkage. Another recent theoretical investigation on oxometal complexes is that of Cundari and co-workers.[12a] By using an effective core potential (ECP) approach within the Hartree−Fock (HF) formalism, the authors have studied some rhenium−oxo complexes with the aim of understanding their electronic structure and chemical reactivity.

In the present investigation, we extend the recent work of Ziegler and Li[14] from the chromium triad to all transition metals in groups 5−8. Methanol is again chosen as the organic substrate, due to the fact that it is the simplest organic species containing both C−H and O−H bonds. The model compounds used in this study are the neutral isoelectronic oxometal species MO_nCl_{4-n} with $n = 1$ for M = V, Nb, Ta, $n = 2$ for M = Cr, Mo, W, $n = 3$ for M = Mn, Tc, Re, and $n = 4$ for M = Fe, Ru, Os. The four elementary processes under investigation are shown in Scheme 1.

The focus of this study has been on the thermochemistry of reactions 1−4. To this end, full geometry optimizations were performed for all the reactants and products of the four processes. Harmonic frequencies were also evaluated for all species, to ensure that the optimized structures corresponded to energy minimum

Scheme 1

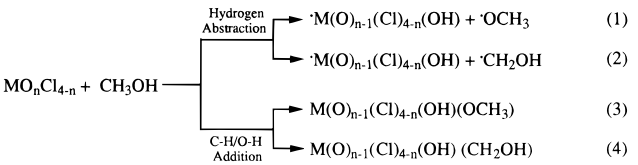

points. The frequencies were further used to estimate zero point energy (ZPE) corrections and thermal contributions to reaction enthalpies and bond strengths.

The objective of our study is (i) to provide structural and thermodynamic data related to the title reactions, (ii) to gain some insight into the energetics of C−H and O−H bond activation of alcohols and alkanes by TM d^0−oxo complexes and (iii) to rationalize the periodic trends in bond strengths and molecular structures within a triad or along a series, with special emphasis on relativistic effects.

We present elsewhere[16] a more detailed kinetic investigation of methanol oxidation by the representative transition metal−oxo species CrO_2Cl_2, MoO_2Cl_2, and RuO_4, in which the overall reaction pathway and activation barriers will be reported. Other studies[17] of chemical reactions based on the same DFT method have appeared previously.

2. Computational Methods

All the reported calculations were carried out by using the Amsterdam Density Functional (ADF) package developed by Baerends *et al.*[18] and vectorized by Ravenek.[19] The numerical integration procedure applied for the calculations is that of te Velde *et al.*[20] An uncontracted triple-ζ STO basis set was used for the *n*s, *n*p, *n*d, $(n + 1)$s, and $(n + 1)$p orbitals of the TM's. For carbon (2s, 2p), chlorine (3s, 3p), oxygen (2s, 2p), and hydrogen (1s), double-ζ basis sets were employed and augmented by an extra polarization function.[21] The inner shells of the first-row TM's (1s2s2p), the second-row TM's (1s2s2p3s3p3d), the third-row transition elements (1s2p-3s3p3d4s4p4d), carbon (1s), and oxygen (1s) as well as chlorine (1s2s2p) were treated by the frozen-core approximation.[14] A set of auxiliary s, p, d, f, and g STO functions were introduced in order to fit the molecular density and Coulomb potential accurately in each SCF cycle.[22] All the geometries and frequencies were calculated at the local density approximation (LDA) level[23] with the parametrization of Vosko *et al.*[24] The relative energies were evaluated by including Becke's nonlocal exchange[25] and Perdew's nonlocal correlation corrections[26] as perturbations based on the LDA density. This approach will be denoted NL-P, and its validity will be discussed later. The

(12) (a) Cundari, T. R.; Conry, R. R.; Spaltenstein, E.; Critchlow, S. C.; Hall, K. A.; Tahmassebi, S. K.; Mayer, J. M. *Organometallics* **1994**, *13*, 322. Some representive work of the semiempirical studies can be found from the references of this paper. (b) Benson, M. T.; Cundari, T. R.; Lim, S. J.; Nguyen, H. D.; Pierce-Beaver, K. *J. Am. Chem. Soc.* **1994**, *117*, 3955.

(13) Russo, T. V.; Martin, R. L.; Hay, P. J.; Rappé, A. K. *J. Chem. Phys.* **1995**, *102*, 9315 and references therein.

(14) Ziegler, T.; Li, J. *Organometallics* **1995**, *14*, 214.

(15) (a) Rappé, A. K.; Goddard, W. A., III. *Nature (London)* **1980**, *285*, 311. (b) Rappé, A. K.; Goddard, W. A., III. *J. Am. Chem. Soc.* **1980**, *102*, 5114. (c) Rappé, A. K.; Goddard, W. A., III. In *Potential Energy Surfaces and Dynamics Calculations;* Truhlar, D. G., Ed.; Plenum: New York, 1981. (d) Rappé, A. K.; Goddard, W. A., III. *J. Am. Chem. Soc.* **1982**, *104*, 448. (e) Rappé, A. K.; Goddard, W. A., III. *J. Am. Chem. Soc.* **1982**, *104*, 3287.

(16) Deng, L.; Ziegler, T. *J. Am. Chem. Soc.*, submitted for publication.

(17) (a) Deng, L.; Ziegler, T.; Fan, L. *J. Chem. Phys.* **1993**, *99*, 3823. (b) Deng, L.; Ziegler, T. *Int. J. Quantum Chem.* **1994**, *52*, 731. (c) Deng, L.; Branchadell, V.; Ziegler, T. *J. Am. Chem. Soc.* **1994**, *116*, 10645. (d) Deng, L.; Ziegler, T. *J. Phys. Chem.* **1995**, *99*, 612.

(18) Baerends, E. J.; Ellis, D. E.; Ros, P. *Chem. Phys.* **1973**, *2*, 41.

(19) Ravenek, W. In *Algorithms and Applications on Vector and Parallel Computers;* te Riele, H. J. J., Dekker, T. J., van de Vorst, H. A., Eds.; Elsevier: Amsterdam, 1987.

(20) (a) Boerrigter, P. M.; te Velde, G.; Baerends, E. J. Int. *J. Quantum Chem.* **1987**, *33*, 87. (b) te Velde, G.; Baerends, E. J. *J. Comput. Phys.* **1992**, *99*, 84.

(21) (a) Snijders, G. J.; Baerends, E. J.; Vernooijs, P. *At. Nucl. Data Tables* **1982**, *26*, 483. (b) Vernooijs, P.; Snijders, G. J.; Baerends, E. J. *Slater Type Basis Functions for the Whole Periodic System*; Internal Report; Free University of Amsterdam: Amsterdam, 1981.

(22) Krijn, J.; Baerends, E. J. *Fit Functions in the HFS-methods;* Internal Report; Free University of Amsterdam, Amsterdam, 1984.

(23) Gunnarson, O.; Lundquist, I. *Phys. Rev.* **1974**, *10*, 1319.

(24) Vosko, S. H.; Wilk, L.; Nusair, M. *Can. J. Phys.* **1980**, *58*, 1200.

(25) Becke, A. D. *Phys. Rev. A* **1988**, *38*, 2398.

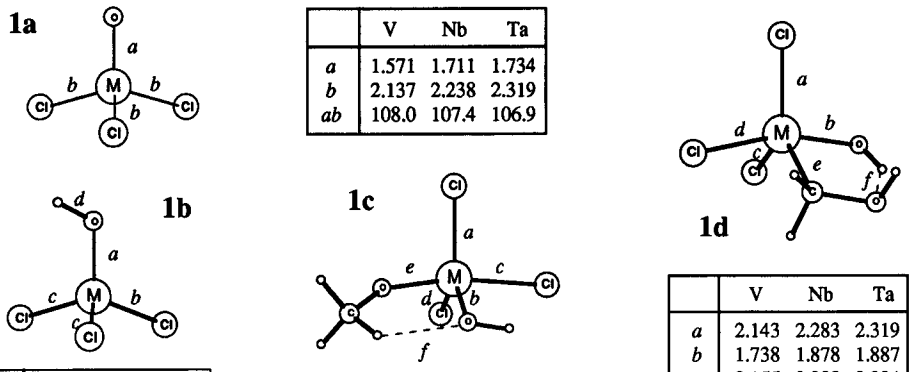

	V	Nb	Ta
a	1.571	1.711	1.734
b	2.137	2.238	2.319
ab	108.0	107.4	106.9

	V	Nb	Ta
a	1.748	1.902	1.905
b	2.135	2.284	2.316
c	2.147	2.292	2.332
d	0.994	0.992	0.996
ab	112.0	116.6	116.0
ac	107.0	105.2	104.6
ad	115.9	117.4	120.2
cab	121.0	120.0	120.0

	a	*b*	*c*	*d*	*e*	*f*
V	2.139	1.799	2.270	2.194	1.749	2.379
Nb	2.294	1.941	2.364	2.297	1.882	2.233
Ta	2.333	1.948	2.432	2.334	1.891	2.231

	ab	*ac*	*ad*	*ae*	*dab*	*eac*
V	120.4	96.8	117.7	98.2	173.7	179.9
Nb	121.4	94.1	115.4	96.5	164.2	178.0
Ta	121.5	93.8	116.7	96.6	162.7	178.0

	V	Nb	Ta
a	2.143	2.283	2.319
b	1.738	1.878	1.887
c	2.155	2.288	2.324
d	2.231	2.341	2.396
e	2.139	2.242	2.264
f	1.576	1.567	1.560
ab	98.4	98.6	98.7
ac	116.5	119.0	119.9
ad	96.9	98.0	98.5
ae	120.5	119.8	119.2
dab	159.0	155.6	154.4
eac	178.0	179.8	179.7

Figure 1. Illustration of the optimized structures of the vanadium triad complexes (bond lengths in angstroms and angles in degrees; M = V, Nb, Ta): **1a**, the reactants; **1b**, the hydrogen abstraction products; **1c**, the O−H bond addition products; **1d**, the C−H bond addition products.

Geometry optimization procedure was based on an analytical gradient scheme developed by Verslius and Ziegler.[27] The harmonic vibrational frequencies were computed from the force constants obtained by numerical differentiation of the energy gradients.[28] Relativistic corrections to the total energy were taken into account by first-order perturbation theory (FO).[29] The extended transition state (ETS) method[30] was applied to analyze the calculated bond energies (BE) for some representative systems. The ETS method decomposes the bond energy, BE, between fragments A and B in the AB molecule

$$\mathrm{BE} = -[\Delta E_{\mathrm{steric}} + \Delta E_{\mathrm{orbit}} + \Delta E_{\mathrm{prep}}] \qquad (5)$$

In the right-hand side of eq 5, the first term is the steric interaction energy between A and B. It can be written as

$$\Delta E_{\mathrm{steric}} = \Delta E_{\mathrm{el}} + \Delta E_{\mathrm{Pauli}} \qquad (6)$$

where ΔE_{el} is the, usually attractive, electrostatic Coulomb interaction between A and B, whereas $\Delta E_{\mathrm{Pauli}}$ is the Pauli repulsion due to the destabilizing two-orbital−four-electron interactions between occupied orbitals on A and B. The term $\Delta E_{\mathrm{orbit}}$ represents the stabilizing interaction between occupied and virtual orbitals on A and B, and ΔE_{prep} takes into account geometrical deformations of A and B as the two fragments are combined into A−B.

3. Results and Discussion

3.1. Structures. Terminal oxometal complexes are known for all metals in group 5 through group 8. An excellent review containing over 600 structurally characterized oxometal complexes can be found in a book by Nugent and Mayer.[2b] Cundari and co-workers[12b] as well as Russo *et al.*[13] have recently reported calculated geometries and frequencies for **1a**, **2a**, and **3a** based on the HF-ECP method. Russo *et al.*[13] have reviewed results from previous computational studies of structures and frequencies for oxometal complexes. The large body of experimental data on the structure and vibrational spectra of oxometal complexes enables us to validate the DFT scheme employed in the present study. Figures 1−4 display the optimized structures for the species involved in reactions 1−4. All the reported geometries represent the lowest energy structure among a number of possible conformations. We shall in this part first compare our structural parameters to the best available experimental and theoretical values. Special emphasis will be put on the sensitivity of the M=O bond length to the chemical environment and electron correlation.[12b]

Vanadium Triad. The reactant $M(O)Cl_3$ (**1a**) has C_{3v} symmetry, whereas the abstraction product MCl_3-OH (**1b**) has a C_s structure with the O−H and M−Cl bonds staggered. The products from respectively O−H (**1c**) and C−H (**1d**) addition have trigonal-bipyramidal (TBP) geometries without symmetry. In **1c** the OCH_3 and Cl groups occupy the axial positions, whereas the axial ligands in **1d** are OH and Cl. A gas-phase electron diffraction (ED) study[31] and HF-ECP calculations[12b,32] afford for $V(O)Cl_3$: R(V−O) = 1.56(4) Å (1.50 Å, HF-ECP); R(V−Cl) = 2.12(3) Å (2.14 Å); ∠OVCl = 108(2)° (109°). The corresponding DFT values at respectively 1.570 Å, 2.134 Å, and 108.0° (Figure 1) display a somewhat better fit to experiment than the HF-ECP results. This is especially true for the V=O linkage, where the HF-ECP bond length is too short by 0.06 Å whereas DFT comes within 0.01 Å of experiment.

(26) (a) Perdew, J. P. *Phys. Rev. Lett.* **1985**, *55*, 1655. (b) Perdew, J. P. *Phys. Rev. B* **1986**, *33*, 8822. (c) Perdew, J. P.; Wang, Y. *Phys. Rev. B* **1986,** *33*, 8800.

(27) Verluis, L.; Ziegler, T. *J. Chem. Phys.* **1988**, *88*, 322.

(28) Fan, L.; Versluis, L.; Ziegler, T.; Baerends, E. J.; Ravenek, W. *Int. J. Quantum Chem. Symp.* **1988**, *22*, 173.

(29) (a) Snijders, J. G.; Baerends, E. J.; Ros, P. *Mol. Phys.* **1978**, *36*, 1789. (b) Snijders, J. G.; Baerends, E. J.; Ros, P. *Mol. Phys.* **1979**, *38*, 1909.

(30) (a) Ziegler, T.; Rauk, A. *Theor. Chim. Acta* **1977**, *46*, 1. (b) Ziegler, T. In *Metal-Ligand Interactions: from Atoms, to Clusters, to Surfaces;* Salahub, D. R., Russo, N., Eds.; NATO ASI Series C378; Kluwer Academic: Dordrecht, The Netherlands, 1992.

(31) Palmer, K. J. *J. Am. Chem. Soc.* **1938**, *60*, 2360.

(32) We have chosen the HF-ECP results of Cundari *et al.* for comparison, because they employed a better basis set than Russo *et al.* did.

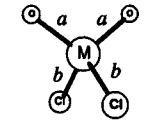

2a

	Cr	Mo	W
a	1.568	1.705	1.731
b	2.105	2.252	2.310
aa	108.4	106.7	105.5
bb	111.6	112.1	113.7

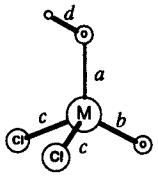

2b

	Cr	Mo	W
a	1.737	1.889	1.916
b	1.556	1.694	1.721
c	2.124	2.264	2.324
d	0.993	0.990	0.991
ab	114.2	117.3	116.9
ac	109.2	108.7	108.8
ad	113.6	117.1	119.0
cab	123.4	125.0	125.7

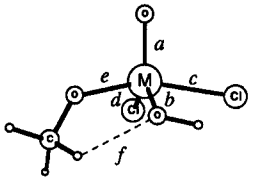

2c

	a	*b*	*c*	*d*	*e*	*f*
Cr	1.555	1.807	2.243	2.175	1.764	2.241
Mo	1.695	1.946	2.332	2.289	1.881	2.147
W	1.722	1.968	2.399	2.347	1.905	2.220

	ab	*ac*	*ad*	*ae*	*dab*	*eac*
Cr	116.8	98.3	114.2	98.6	179.8	172.8
Mo	114.8	99.8	110.0	100.3	178.8	167.8
W	112.7	101.9	110.8	100.9	178.5	168.3

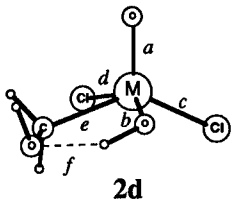

2d

	Cr	Mo	W
a	1.557	1.696	1.732
b	1.742	1.868	1.893
c	2.161	2.286	2.343
d	2.190	2.309	2.370
e	2.143	2.229	2.261
f	1.603	1.548	1.563
ab	105.4	101.9	101.5
ac	113.4	116.6	117.2
ad	104.9	101.8	102.0
ae	98.9	107.1	107.5
dab	157.0	154.9	154.1
eac	179.7	179.9	179.9

Figure 2. Illustration of the optimized structures of the chromium triad complexes (bond lengths in angstroms and angles in degrees; M = Cr, Mo, W): **2a**, the reactants; **2b**, the hydrogen abstraction products; **2c**, the O−H bond addition products; **2d**, the C−H bond addition products.

	Mn	Tc	Re
a	2.096	2.228	2.296
b	1.570	1.707	1.742
ab	108.5	109.5	110.2

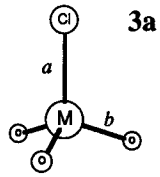

3a

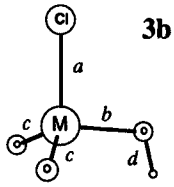

3b

	Mn	Tc	Re
a	2.104	2.241	2.308
b	1.565	1.706	1.741
c	1.740	1.896	1.932
d	0.993	0.990	0.991
ab	111.0	111.7	112.4
ac	99.4	96.4	94.1
bd	109.9	110.2	111.4
cab	115.5	113.9	113.5

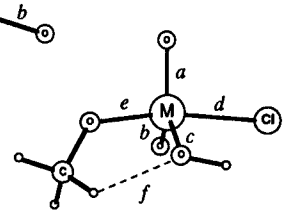

3c

	a	*b*	*c*	*d*	*e*	*f*
Mn	1.562	1.569	1.760	2.461	1.745	2.260
Tc	1.704	1.710	1.946	2.344	1.888	2.082
Re	1.738	1.743	1.981	2.401	1.917	2.081

	ab	*ac*	*ad*	*ae*	*cab*	*ecd*
Mn	115.3	122.2	78.5	105.9	150.5	175.8
Tc	112.2	124.9	95.1	98.1	175.0	179.5
Re	111.8	124.7	95.2	98.9	174.0	178.7

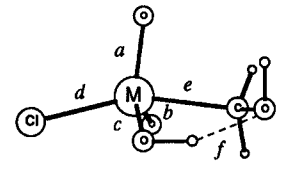

3d

	Mn	Tc	Re
a	1.573	1.708	1.743
b	1.568	1.713	1.749
c	1.792	1.919	1.949
d	2.164	2.284	2.351
e	2.190	2.229	2.258
f	1.807	1.680	1.682
ac	115.3	113.0	112.2
bc	120.9	125.7	127.0
dc	83.2	81.7	81.4
ec	79.0	75.7	75.5
cab	148.9	153.2	153.1
ecd	176.3	168.4	165.5

Figure 3. Illustration for the optimized structures of the manganese triad complexes (bond lengths in angstroms and angles in degrees; M = Mn, Tc, Re): **3a**, the reactants; **3b**, the hydrogen abstraction products; **3c**, the O−H bond addition products; **3d**, the C−H bond addition products.

The $Nb(O)Cl_3$ fragment has been characterized by X-ray crystallography in the adducts $NbOCl_3L_2$ (L = MeCN, $OP(NMe_2)_3$ (hmpa)).[33] The DFT-predicted Nb=O bond length of 1.711 Å falls into the range of the experimental data (1.68(2) Å in the MeCN adduct, 1.692(5) Å in the hmpa adduct, and 1.71(3) Å in a $NbO(S_2CNEt_2)_3$ complex). Our calculated Ta=O bond length in $TaOCl_3$ of 1.734 Å is also in good agreement with the only available measured Ta−O distance (1.725(7) Å, in $TaO(N(i\text{-}Pr)_2)_3$) for monooxo complexes. By comparison, the HF-ECP method affords again M=O distances that are too short (1.65 Å for Nb=O and 1.67 Å for Ta=O). The LDA and HF-ECP results for M−Cl bond lengths of **1a** are essentially the same, in the case of $VOCl_3$, and both methods reproduced the experimental data. The HF-ECP method assigns a length of 2.31 Å to both Nb−Cl and Ta−Cl bonds, whereas the LDA scheme affords 2.238 Å for Nb−Cl and 2.319 Å for Ta−Cl. The LDA results for Nb−Cl bond lengths in the complexes **1a**−**d** range from 2.284 to 2.364 Å (Figure 1), consistent with the experimental data for the terminal Nb−Cl bonds in $(NbCl_5)_2$ (2.250(6) and 2.302 Å) and in $NbOCl_3(MeCN)_2$ (2.313(9)−2.377(8) Å).[2b]

A tentative assessment of the relative metal−ligand bond strengths can be drawn from the structural data of Figure 1 by comparing the M−X (X = C, Cl, O) distances with the sum of the covalent radii for the atoms involved. Taking the vanadium system as an example, the single-bond distances of the V−X linkage as estimated from the sum of the covalent radii are 1.99, 2.21, and 1.95 Å for X = C, Cl, and O respectively. The

(33) (a) Chavant, C.; Daran, J. C.; Jeannin, Y.; Constant, C.; Marancho, R. *Acta Crystallogr., Ser. B* **1975**, *31*, 1828. (b) Hubert-Pfalzgraf, L. G.; Pinkerton, A. A. *Inorg. Chem.* **1977**, *16*, 1895.

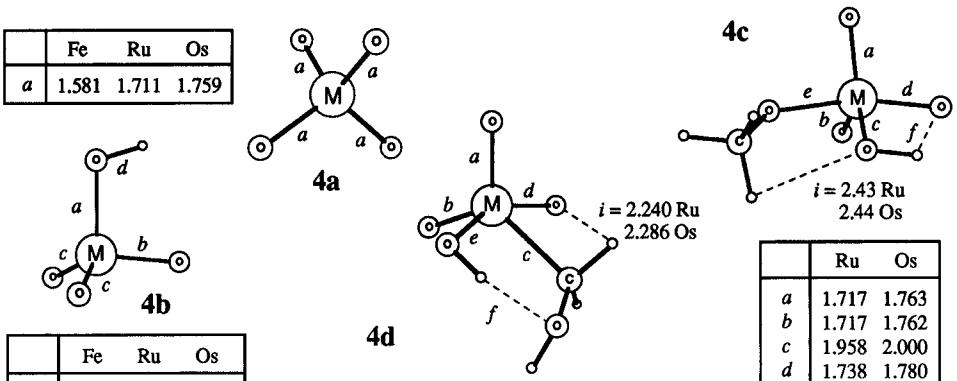

	Fe	Ru	Os
a	1.581	1.711	1.759

	Fe	Ru	Os
a	1.736	1.883	1.931
b	1.602	1.744	1.794
c	1.572	1.707	1.758
d	0.994	0.997	0.995
ab	98.3	96.0	93.9
ac	109.4	110.0	110.8
ad	104.9	106.2	106.8
cab	116.2	113.8	112.4

	a	*b*	*c*	*d*	*e*	*f*
Ru	1.716	1.716	2.230	1.748	1.930	1.683
Os	1.763	1.763	2.250	1.793	1.967	1.686

	ac	*bc*	*dc*	*ec*	*cab*	*ecd*
Ru	119.3	122.5	71.4	76.5	171.7	178.6
Os	119.2	122.1	71.9	76.3	171.4	178.8

	Ru	Os
a	1.717	1.763
b	1.717	1.762
c	1.958	2.000
d	1.738	1.780
e	1.945	1.980
f	1.979	2.040
ac	123.1	123.2
bc	124.1	124.1
dc	79.9	79.8
ec	74.9	74.5
cab	166.7	167.2
ecd	179.6	179.7

Figure 4. Illustration of the optimized structures of the iron triad complexes (bond lengths in angstroms and angles in degrees; M = Fe, Ru, Os; **4a**, the reactants; **4b**, the hydrogen abstraction products; **4c**, the O−H bond addition products; **4d**, the C−H bond addition products (for M = Fe, no hydrogen addition products were found).

Calculated bond lengths for V−Cl of **1a**−**d** are 2.137−2.270 Å, indicating a single bond. On the other hand, the V−C distance of 2.155 Å in **1d** is much longer than the estimated single-bond length (1.99 Å), which implies that the V−C bond of **1d** is rather weak. The V=O linkage of four-coordinate monooxo complexes is usually considered as a triple bond.[2b] The theoretical bond lengths of V−OH and V−OCH_3 in **1b**−**d** are 1.738−1.779 Å, lying between the length of a triple bond (1.571 Å) and a single bond (approximately 1.99 Å). Thus, the V−OH and V−OCH_3 linkages can be expected to have some multiple-bonding character resulting from, as we shall show later, the donation of electron density from the oxygen lone-pair orbitals to the electron-deficient metal d orbitals. Further, the V−OCH_3 distance is shorter than that of the corresponding V−OH bond length, indicating a stronger bond in the former case. Also noticeable in Figure 1 is the trans influence. Thus, the lengths of M−Cl bonds trans to OCH_3 and OH ligands are larger than cis M−Cl bonds. Furthermore, the trans-influence of OCH_3 is seen to be stronger than that of OH.

Chromium Triad. Among the transition metal d^0−oxo complexes, those of group 6 elements have been the most extensively studied. The optimized structures in Figure 2 are C_{2v} for **2a**, C_s for **2b**, and C_1 for **2c** as well as **2d**. Gas-phase ED studies[29,34] of CrO_2Cl_2 have determined[32] with high accuracy that R(Cr−O) = 1.581(2) Å, R(Cr−Cl) = 2.126(2) Å, ∠OCrO = 108.5(4)°, and ∠ClCrCl = 113.3 (3)°. The corresponding LDA (Figure 2a) and HF-ECP values[12b] are 1.568 Å (1.50 Å, HF-ECP), 2.105 Å (2.12 Å), 108.4° (109°), and 111.6° (109°), respectively. It is clear that the LDA geometry compares better with the experimental structure than the HF-ECP geometry. Thus, the largest LDA deviation amounts to 0.015 Å for the Cr−Cl bond, whereas HF-ECP is short by 0.08 Å for the Cr=O bond. For bond angles, the maximum deviation is 1.3° in the case of LDA compared to 4° for the HF-ECP scheme.

The experimental[35] structure for MoO_2Cl_2 carries a considerable uncertainty with R(Mo−O) = 1.75(10) Å and R(Mo−Cl) = 2.28(3) Å. Fortunately, a large number of monooxo- and *cis*-dioxomolybdenum complexes have been structurally characterized by crystallographic studies. The Mo−O distances in both monooxo and *cis*-dioxo complexes are found to fall in a narrow Gaussian distribution, with the standard deviations being less than 0.015 Å.[2b] The expectation values for M−O are 1.675 and 1.705 Å for monooxo and *cis*-dioxo species, respectively. The DFT results of Mo−O in **2b**−**d** are about 1.695 Å for the monooxo species and 1.705 Å for dioxo species **2a**. Thus, both compare favorably with the experimental estimates.

The structural tables of Nugent and Mayer contain only two d^0−oxo complexes, $WO_2Cl_2(OPPh_3)_2$ and $W(O)_2Cl_2$(acac), with a WO_2Cl_2 framework. The W−O bond lengths are 1.702(9) and 1.706(8) Å for the former and 1.716(5) and 1.723(5) Å for the latter. The corresponding LDA value of 1.731 Å for **2a** somewhat seems to overestimate the W−O bond lengths, yet it is still in reasonable agreement with the experimental data. The HF-ECP estimates for R(M−O) of 1.64 Å in the case of MoO_2Cl_2 and 1.66 Å for WO_2Cl_2 are again seen to be too short.

It follows from Figure 2 that the limiting conformation for **2c**,**d** is square pyramidal (SP) with oxygen occupying the apical position in order to maximize the p_π−d_π overlaps between orbitals on oxygen and the metal center. As a result, the M−O bond lengths in **2c**,**d** are slightly shorter than those in **2a**. The M−OCH_3 bond is again seen to be shorter than the M-OH linkage and to exert a stronger trans influence on the M−Cl distance. Both factors are attributed to a considerable p_π−d_π interaction in the M−OCH_3 bond.

Manganese Triad. The optimized structures for the trioxo complexes MO_3Cl (M = Mn, Tc, Re) have C_{3v} symmetry with three oxygens in the facial positions. Structural parameters for ReO_3Cl have been determined by microwave spectroscopy[36] as R(Re−O) = 1.702(3) Å,

(34) Marsden, C. J.; Hedberg, K. *Inorg. Chem.* **1982**, *21*, 1115.

(35) Skinner, H. A. *Chem. Soc.-Spec. Publ.* **1958**, *No. 11*, M80.

Table 1. Comparison of M−O Stretching Frequencies for Oxometal Complexes[a]

	$VOCl_3$	CrO_2Cl_2		MoO_2Cl_2		WO_2Cl_2		ReO_3Cl		RuO_4		OsO_4	
method	a_1	a_1	b_1	a_1	b_1	a_1	b_1	a_1	b_1	a_1	t_2	a_1	t_2
exptl[b]	1043	991	1002	994	972	992	985	1001	960	882	914	965	961
LDA[c]	1090	1056	1078	986	968	978	941	957	922	920	953	910	895
HF-ECP[d]	1285	1263	1169	1134	1067	1130	1065					1103	1023
HF-ECP[e]	1286	1238		1138		1140		1134		899		1093	

[a] Units in cm^{-1}. Legend: a_1, symmetric stretching; b_1, asymmetric stretching. [b] Cited from ref 2b. [c] This work. [d] Reference 13. [e] Reference 12b.

R(Re−Cl) = 2.229(4) Å, and ∠OReCl = 109.4(1)°. Our optimized bond lengths (Figure 3a) are 1.742 and 2.296 Å, longer than the experimental data by 0.040 and 0.067 Å, respectively. The HF-ECP method, on the other hand, underestimates the Re−O bond length by 0.042 Å while it overestimates the Re−Cl bond length by 0.051 Å. The discrepancies between calculated and measured OReCl angles are 0.8 and −1.4° for the LDA and HF-ECP methods, respectively. Our calculations on MnO_3Cl cannot be directly compared to experiment, since diffraction data are lacking for this system. Accurate data[33] are available for MnO_3F with R(Mn−O) = 1.586(5) Å and ∠OMnF = 108.5(1)°. By extrapolating from experimental differences in the structures of ReO_3F and ReO_3Cl, we come to the experimental estimates of R(Mn−O) = 1.595 Å and ∠OMnCl = 108.5° for MnO_3Cl. The LDA results (Figure 3) are in good agreement with these data. In contrast, the HF-ECP value of 1.51 Å for the Mn=O bond length in MnO_3F is significantly (0.076 Å) shorter than experiment. It has been found[12b] that the amount of electron correlation required to describe correctly multiple bonds between transition metals and main group elements increases from bottom to top within a triad. This is the reason the HF-ECP scheme fares worse for the 3d systems than for the heavier homologues. On the other hand, DFT seems to provide smaller and more uniform errors since it already includes correlation to some degree.

The optimized structures for **3b** are of C_s symmetry. The ratio between the M−OH bond lengths and the M=O bond distances is similar to that calculated for **2b**, indicating that the M−OH linkages involves in part double bonds. The double-bond character can be attributed to an interaction between the lone-pair p_π oxygen orbital on the hydroxyl group and a d_π orbital on the metal. This $p_\pi-d_\pi$ interaction is optimal for the C_s symmetry. Both **3c** and **3d** are trigonal-bipyramidal (TBP) structures with respectively CH_2OH and OCH_3 in the axial position opposite the least trans directing group, Cl. The hydroxymethyl complex **3d** has a strong hydrogen bond between the OH ligand and the oxygen on the hydroxymethyl group.

Iron Triad. Oxometal complexes of ruthenium and osmium are abundant and have been used in many different fields of chemistry. The corresponding iron complexes have in many cases not been isolated. We are only aware of a few structurally characterized monooxo complexes of iron.[2b]

Gas-phase ED studies[37] have shown that RuO_4 and OsO_4 are of T_d symmetry with M=O bond lengths of 1.705(3) and 1.711(3) Å for M = Ru[37a] and M = Os,[37b] respectively. The corresponding FeO_4 system is not known. Our LDA value of 1.711 Å for the Ru−O bond is in excellent agreement with the experimental date. The LDA bond length for Os-O is 0.048 Å longer than the experimental estimate. The HF-ECP scheme assigns a value of 1.66 Å to both the Ru=O and Os=O bond lengths. We notice again that the HF-ECP method underestimates M=O bond distances.

It is interesting to note that the optimized structure for the hydrogen abstraction products **4b** has C_s symmetry with an eclipsed conformation in which the hydroxyl hydrogen forms a week interaction to the oxygen of the cis M−O bond. The related group 6 compound **2b** adopts on the other hand a staggered conformation, also of C_s symmetry. The cis oxygen in **4b** is relatively electron rich, with three oxygen atoms competing as π donors. For this reason, further electron donation from oxygen is possible through hydrogen bonding. The single oxygen π acceptor in **2b** is electron poor and not available for further electron donation. Thus, the OH bond in **2b** adopts the conformation with the lowest steric interaction energy. In **4c** the preferred conformation is C_1 with one M−O bond coplanar with the OH linkage, again indicating some hydrogen bonding. It should also be mentioned that the M=O bond distance increases within the same transition series from left to right, although the metal radius decreases. The trend reflects again that the π donation and multiple-bonding character for each M=O bond diminishes as more competing oxygen atoms are added to the same metal center. We note also that the M-OH and M-OCH_3 bonds experience a similar trend, again indicating a decrease in π bonding from left to right in a series.

3.2. Stretching Frequencies for M−O Bonds of the Oxometal Complexes. Table 1 compares available gas-phase data on M−O stretching frequencies for terminal oxometal complexes with theoretical estimates. This comparison helps us further to assess how well our theoretical model can describe multiple M−O bonds.

It follows from Table 1 that the LDA frequencies compare much better with experimental data than the HF-ECP values. Thus, the rms deviations are 4.8% for LDA as compared to 16.2% for the HF-ECP scheme. The largest absolute discrepancies between theoretical and measured data are respectively 66 cm^{-1} for LDA in the case of OsO_4 and 272 cm^{-1} for HF-ECP in the case of CrO_2Cl_2. The accuracy of the LDA frequencies calculated here for the M−O stretches appears to be similar to that for systems containing main group elements[17,38ae] and transition metals.[38b−d,f]

(36) Lotspeich, J. F.; Javan, A.; Englebrecht, A. *J. Chem. Phys.* **1959**, *31*, 633.

(37) (a) Schafer, L.; Seip, H. M. *Acta Chem. Scand.* **1967**, *21*, 737. (b) Seip, H. M.; Stolevik, R. *Acta Chem. Scand.* **1966**, *20*, 385.

(38) (a) Fan, L.; Ziegler, T. J. Chem. Phys. **1992**, 96, 9005. (b) Fan, L.; Ziegler, T. *J. Phys. Chem.* **1992**, *96*, 6937. (c) Berces, A.; Ziegler, T. *J. Phys. Chem.* **1994**, *98*, 13233. (d) Berces, A.; Ziegler, T. *J. Phys. Chem.* **1995**, *99*, 11417. (e) Berces, A.; Ziegler, *T. J. Chem. Phys.* **1993**, *98*, 4793. (f) Deeth, R. J. *J. Phys. Chem.* **1993**, *97*, 11625.

Table 2. Reaction Enthalpies (kcal/mol) for the O−H and C−H Bond Activation Processes (1)−(4)[a]

group	transition metal	H abstraction from O−H					H abstraction from C−H					O−H bond addition					C−H bond addition				
		ΔE	ΔE_r	ΔZPE	$\Delta\Delta H$	$\Delta H°_{298}$	ΔE	ΔE_r	ΔZPE	$\Delta\Delta H$	$\Delta H°_{298}$	ΔE	ΔE_r	ΔZPE	$\Delta\Delta H$	$\Delta H°_{298}$	ΔE	ΔE_r	ΔZPE	$\Delta\Delta H$	$\Delta H°_{298}$
VA	V	57.0	1.30	−4.53	0.66	54.4	50.2	1.41	−3.30	0.96	49.3	7.5	0.07	0.93	−0.42	8.1	31.3	0.50	0.96	−0.62	32.1
	Nb	70.8	2.85	−4.35	0.59	69.9	64.0	2.96	−3.12	0.89	64.7	−8.1	−1.80	1.18	−0.36	−9.1	22.5	−0.24	1.10	−0.67	22.7
	Ta	72.7	7.68	−4.45	0.61	76.5	65.9	7.78	−3.22	0.91	71.4	−7.7	−3.60	1.07	−0.32	−10.6	21.8	0.56	1.02	−0.66	22.7
VIA	Cr	41.3	0.60	−4.31	0.61	38.2	34.6	0.71	−3.08	0.91	33.1	8.2	0.50	0.69	−0.47	8.9	23.0	−0.01	1.20	−0.57	23.6
	Mo	57.6	3.68	−4.22	0.59	57.5	51.0	3.74	−2.99	0.89	52.6	−2.2	−1.07	0.98	−0.35	−2.6	17.9	0.26	1.29	−0.66	18.8
	W	60.2	8.82	−4.23	0.59	64.4	53.4	8.91	−3.00	0.89	60.2	−4.9	−3.24	0.90	−0.30	−7.5	15.2	−0.03	1.48	−0.72	15.9
VIIA	Mn	29.9	1.47	−4.23	0.64	27.8	23.1	1.57	−3.00	0.94	22.6	9.7	0.87	0.37	−0.35	10.6	8.4	1.44	1.71	−0.45	11.1
	Tc	46.6	3.92	−4.08	0.58	47.0	39.8	4.02	−2.85	0.88	41.9	4.7	0.09	0.86	−0.31	5.3	12.7	1.41	1.84	−0.56	15.4
	Re	51.2	8.10	−4.06	0.57	55.8	44.4	8.20	−2.83	0.87	50.6	2.1	−1.35	0.85	−0.26	1.3	11.8	0.87	1.83	−0.56	13.9
VIIIA	Fe	17.9	1.83	−3.91	0.47	16.3	11.1	1.93	−2.68	0.77	11.1										
	Ru	36.4	5.44	−3.95	0.48	38.4	29.6	5.57	−2.72	0.78	33.2	14.4	2.00	1.10	−0.45	17.1	14.7	3.31	1.49	−0.48	19.0
	Os	42.6	10.99	−3.88	0.47	50.2	35.8	11.10	−2.65	0.77	45.0	9.9	1.88	1.29	−0.46	12.6	12.8	4.00	1.67	−0.57	17.9

[a] Legend: ΔE, the nonrelativistic electronic enthalpy; ΔE_r, relativistic corrections; ΔZPE, zero point energy correction; $\Delta\Delta H$, thermal correction (see text for details); $\Delta H°_{298}$, the reaction enthalpy at 298.15 K.

Table 3. MO−H Bond Strengths (kcal/mol)[a]

	VA			VIA			VIIA			VIIIA		
	V	Nb	Ta	Cr	Mo	W	Mn	Tc	Re	Fe	Ru	Os
ΔE	50.8	37.0	35.1	66.5	50.1	47.4	77.9	61.2	56.6	89.9	71.4	65.2
ΔE_r	−1.41	−2.98	−7.83	−0.80	−3.82	−8.79	−1.61	−4.07	−8.24	−1.97	−5.60	−11.13
ΔZPE	−5.49	−5.67	−5.57	−5.71	−5.80	−5.79	−5.79	−5.94	−5.96	−6.11	−6.07	−6.14
$\Delta\Delta H$	0.77	0.84	0.82	0.82	0.84	0.84	0.79	0.85	0.86	0.96	0.95	0.96
$\Delta H°_{298}$	44.7	29.2	22.5	60.8	41.3	33.7	71.3	52.0	43.3	82.8	60.7	48.9

[a] Legend: ΔE, the electronic enthalpy; ΔE_r, relativistic corrections; ΔZPE, zero point energy correction; $\Delta\Delta H$, thermal correction (see text for details); $\Delta H°_{298}$, the reaction enthalpy at 298.15 K.

A further examination of the results in Table 1 reveals that the LDA frequencies are consistently higher than the experimental data for the first-row TM complexes. This is related to the fact that the LDA method underestimates the M−O bond distances for 3d elements. As was most recently discussed by Berces and Ziegler,[38d] the reference geometry at which frequencies are evaluated strongly influences the theoretical estimates, and bond distances that are too short afford stretching frequencies that are too high. For the third-row TM systems, the M−O distances determined by LDA are too long, and the M−O frequencies as a consequence[38d] are too low. The best agreement is obtained for the second-row TM systems, where LDA affords the best fit to experimental M−O distances.

Deeth[38f] has reported the nonlocal M-O stretching frequencies as 986 (a_1) and 991 (b_1) cm^{-1} for CrO_2Cl_2. The corresponding estimates for MoO_2Cl_2 are 914 (a_1) and 897 (b_1) cm^{-1}. The nonlocal corrections are seen to reduce the LDA frequencies as[38d] they systematically increase the calculated M−O distances. This is beneficial for the first-row TM complexes. However, nonlocal corrections makes the fit to experimental frequencies worse for second-row and third-row TM compounds by elongating the already overestimated LDA M-O distances. We shall discuss this point further in section 3.4.

3.3. Thermodynamic Properties. Reaction Enthalpies. Table 2 summarizes the calculated reaction enthalpies, ΔH_{298}, for the processes (1)−(4). At the applied level of theory, ΔH_{298} is

$$\Delta H°_{298} = \Delta E + \Delta E_r + \Delta\mathrm{ZPE} + \Delta(\Delta H°_{298} - \Delta H°_0) \quad (7)$$

where ΔE is the non-elativistic electronic reaction enthalpy, ΔE_r is the relativistic correction to ΔE based on the first-order (FO) perturbation theory, ΔZPE is the relative vibrational zero-point energy estimated from the harmonic frequencies; and the last term, $\Delta(\Delta H°_{298} - \Delta H°_0) = \Delta\Delta H$, is the thermal correction which may consist of translational, rotational, and pV work as well as vibrational contributions.[17c] The term $\Delta\Delta H$ was calculated by standard statistical thermodynamic methods based on the rigid rotor−harmonic oscillator model. For reactions 1 and 2 the term $\Delta\Delta H$ contains only a vibrational component. For the O−H and C−H bond addition processes (3) and (4), $\Delta\Delta H$ includes in addition contributions from the work term $pV = -RT$ (−0.593 kcal/mol), three added degrees of translation (−(3/2)-RT = −0.890 kcal/mol), and three added degrees of rotation (−(3/2)RT = −0.890 kcal/mol).

Table 4. Population Analyses of M−OCH_3 and M−CH_2OH Bonds for M = Cr, Mo, W, Ru

	M−OCH_3				M−CH_2OH	
	σ		π		σ	
M	M	OCH_3	M	OCH_3	M	CH_2OH
Cr	0.54	1.46	0.36	1.64	0.95	1.05
Mo	0.44	1.56	0.33	1.67	0.82	1.18
W	0.41	1.59	0.34	1.66	0.80	1.20
Ru	0.57	1.43	0.24	1.76	1.10	0.90

For each TM atom, the endothermicity of the four reactions follows the same order: O−H hydrogen abstraction > C−H hydrogen abstraction > C−H bond addition > O−H bond addition. The addition reaction gives rise to one extra bond. Thus, it is not surprising that it is less endothermic than the abstraction processes with a net loss of a single bond. Further, for the abstraction the stronger O−H bond is harder to activate. On the other hand, C−H is most difficult to activate by the addition process, since the M−OCH_3 bond formed from the addition of O−H is much stronger than the M−CH_2OH bond formed from C−H addition (Tables 3 and 4). From the large enthalpy difference between processes 1 and 3, one may expect that O−H bond cleavage proceeds exclusively through the addition

pathway. On the other hand, C−H activation can proceed through abstraction as well as addition, with a preference given to the latter pathway. We shall show elsewhere[16] that these conclusions hold as well when activation barriers are taken into account.

The enthalpies given in Table 2 exhibit clear periodic trends. For the hydrogen abstraction process, the endothermicity is seen to decrease on going from bottom to top in a triad and from left to right within a transition series. The determining factor here is an increase in the MO−H bond strength following the same direction (Table 3). We shall explain the reason for the periodic variation in the MO−H bond strength shortly.

The endothermicity of the addition processes follows the exact opposite trend with an increase from bottom to top in a triad and from left to right within a transition series (Table 2). The determining factor is now the tendencies in the M−OCH_3 and M−CH_2OH bond energies. Both bonds are seen to be stronger for the heavier congener in a triad and for the later metals in a series (Table 4). Again, we shall analyze trends in the M−OCH_3 and M−CH_2OH bond energies in more detail later.

The results compiled in Table 2 would indicate that oxo complexes of late to middle metals in the first transition series, such as iron or manganese, would be the best candidates for activation of C−H (or O−H) bonds by abstraction. On the other hand, oxo complexes of early metals in the third transition series are in the best position to activate O−H bonds by addition.

We note further that early transition metals of group 5 and group 6 elements are more likely to add the stronger O−H bond than the weaker C−H linkage. This is so since the cost of breaking the stronger O−H bond is more than compensated for by forming a M−OCH_3 bond that is much stronger than the M−CH_2-OH linkage (Table 4). The compensation is not as large for the middle to late transition metals, since the difference in the M−OCH_3 and M−CH_2OH bond energies are smaller here (Table 4). For this reason, O−H and C−H additions have similar reaction enthalpies for oxo complexes of group 7 and group 8 metals.

There have been some experimental studies on activation of O−H and C−H bonds by oxo complexes where the addition mechanism is assumed to be operative. These investigations tried to assess the relative preference for O−H addition over C−H addition by comparing rates for oxidation of alcohols and ethers.[7b] For oxo complexes in which O−H addition is much faster, only alcohol should be oxidized, whereas both alcohol and ether are oxidized for systems where both O−H and C−H addition are feasible.

The experimental studies revealed that chromic acid oxidizes alcohols much faster than ethers.[39] Thus, chromium seems to prefer O−H over C−H addition, in agreement with our findings (Figure 2). On the other hand, ruthenium tetraoxide[10b] and permanganate[7b] as well as ferrate[8a] are found readily to oxidize both alcohols and ethers. Thus, for these centers both O−H and C−H addition are likely, again in agreement with our calculations (Figure 2).

Many of the arguments presented here have depended on periodic changes in the MO−H, M−OCH_3, and M−CH_2OH bond dissociation energies. We shall in the following give an analysis of the factors responsible for these changes.

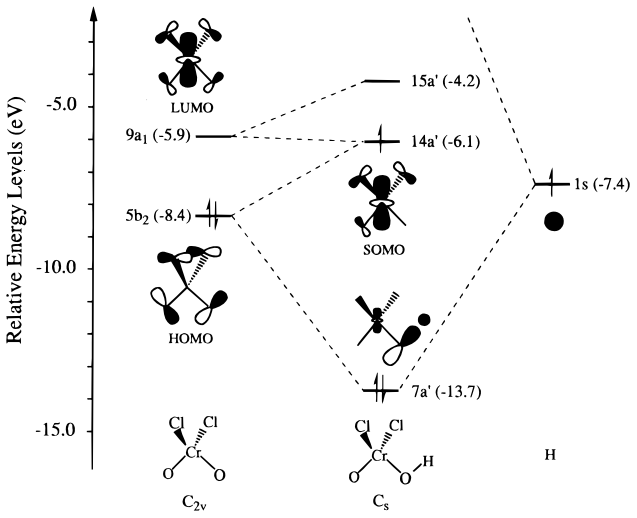

Figure 5. Orbital interaction diagram for the formation of the $Cr(O)(Cl)_2O$−H bond.

MO−H Bond Enthalpies of the Hydrogen Abstraction Products. Table 3 displays the MO−H bond enthalpies, ΔH_{298}, along with the individual components contributing to ΔH_{298}. The strength of the MO−H bond is important, since it completely determines how the reaction enthalpies for the hydrogen abstraction processes (1) and (2) are influenced by the metal center. Thus, the stronger the MO−H bond, the smaller (less endothermic) the enthalpy for the abstraction reactions. We shall now provide a detailed analysis of how ΔH_{298} for the MO−H bond changes with the metal center in order to explain the periodic trends for the abstraction enthalpies reported in Tables 1 and 2.

The MO−H bond can be considered as formed from a three-orbital−three-electron interaction between the hydrogen atom and the oxometal complex, as illustrated for $CrCl_2(OH)(O)$ in Figure 5. The orbitals involved are the HOMO and LUMO of the oxometal complex, here $CrCl_2O_2$, as well as the singly occupied (SO) 1s orbital on hydrogen. The HOMO is ligand-based with out-of-phase contributions from the p_π lone-pair orbitals. For $CrCl_2O_2$ the $5b_2$ HOMO has a composition of $2p_O$ (65%) + $3p_{Cl}$ (35%) (Figure 5). The LUMO is primarily a d_{z^2} metal orbital with antibonding contributions from p_π on the ligands. For the $9a_1$ LUMO of $CrCl_2O_2$ the composition is d_{z^2} (58%) + $3p_{Cl}$ (24%) + $2p_O$ (18%) (Figure 5).

The interaction between the oxometal complex and H gives rise to a strongly MO−H bonding orbital with respect to $1s_H$ and the HOMO. This orbital is identified in $CrCl_2(O)(OH)$ as 7a′ (O 2p (76%) + Cr d_{z^2} (12%) + H 1s (12%); Figure 5). The SOMO is, on the other hand, represented as the LUMO of the oxometal complex and given by 14a′ (Cr d_{z^2} (61%) + Cl 3p (30%) + O 2p (9%)) in the case of $Cr(O)(Cl)_2OH$. One might view the MO−H bond formation as taking place by the promotion of an electron from the HOMO to the LUMO of the oxometal complex followed by electron pairing of the remaining electron in the HOMO with the single hydrogen electron. Thus, the MO−H bond strength will depend on the stabilization gained in the electron pairing as well as the energy required for the electron promotion.

(39) Brownell, R.; Leo, A.; Chang, Y. W.; Westheimer, F. H. *J. Am. Chem. Soc.* **1962**, *82*, 406.

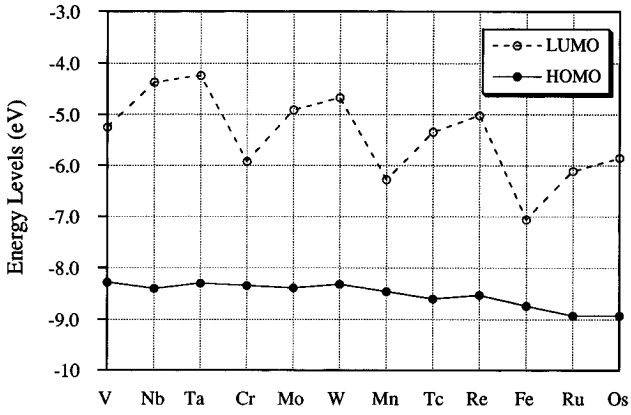

Figure 6. A plot of energy gaps between the HOMO and LUMO for the group 5 to group 8 transition metal d^0−oxo complexes.

Our ETS decomposition analysis shows that the stabilization from the electron pairing is nearly constant for the different oxo complexes, whereas the promotion energy changes with the metal center. The promotion energy, $\Delta E_{HL} = E_{LUMO} - E_{HOMO}$, is the difference between the energy of the HOMO, E_{HOMO}, and the energy of the LUMO, E_{LUMO}. The larger the promotion energy required, the weaker the MO−H bond.

Figure 6 plots E_{HOMO} and E_{LUMO} for the different oxo complexes. It follows from Figure 6 that E_{HOMO} essentially is the same within a given TM triad. For obvious reasons, E_{HOMO} decreases slightly from left to right in Figure 6 as chlorines are substituted by oxygens in the ligand-based HOMO. On the other hand, E_{LUMO} is much more dependent on the metal center. It decreases from bottom to top within a given TM triad and from left to right within a TM series. Thus, trends in the promotion energy as well as the MO−H bond strength are primarily set by E_{LUMO}. That is, the lower the LUMO energy, the stronger the MO−H bond.

The trend in E_{LUMO} is a direct consequence of the ligand−metal antibonding character of the LUMO (Figure 5). Within a triad the metal−ligand overlaps increase down a triad as the d orbitals expand. The expansion makes the LUMO more antibonding and increases its energy (Figure 6). Along a TM series the d orbitals contract from left to right. As a consequence, the LUMO becomes less antibonding and its energy is lowered (Figure 6). In conclusion, the metal with the more diffuse d orbitals forms the weaker MO−H bond and is less likely to abstract a hydrogen from a C−H or O−H linkage. It should be pointed out that our analysis explains why the LUMO in FeO_4 is especially low. In fact, FeO_4 only exists as the reduced derivatives FeO_4^- and FeO_4^{2-}, where one or two electrons have been added to the low-lying LUMO.

Relativity is seen to weaken the MO−H bond. This is understandable since relativistic effects destabilize[40] d orbitals and thus raise the energy of the metal-based LUMO. The increase in E_{LUMO} will in turn weaken the MO−H bond as explained above. The importance of relativity is greatest for the 5d elements, as expected.

(40) (a) Schwarz, W. H. E.; van Wezenbeek, E. M.; Baerends, E. J.; Snijders, G. J. J. *J. Phys. B* **1989**, *22*, 1515. (b) Ziegler, T.; Snijders, J. G.; Baerends, E. J. In *The Challenge of d and f Electrons;* Salahub, D. R., Zerner, M. C., Eds.; American Chemical Society: Washington, DC, 1989.

M−OCH_3 and M−CH_2OH Bond Strengths. The reaction enthalpy for the C−H addition reaction (3) is given by

$$\Delta E_3 = \Delta H(\text{C−H}) - \Delta H(\text{MO−H}) - \Delta H(\text{M−CH}_2\text{OH}) \quad (8)$$

and that of the O−H addition reaction (4) as

$$\Delta H_4 = \Delta H(\text{O−H}) - \Delta H(\text{MO−H}) - \Delta H(\text{M−OCH}_3) \quad (9)$$

We have already seen how the MO−H bond strength influences the periodic trends in the O−H and C−H abstraction enthalpies for (1) and (2). Essentially, ΔH(MO−H) gives rise to a reduction in the endothermicity of (1) and (2) from bottom to top of a TM triad and from left to right of a TM series. The MO−H bond strength would have the same influence on the addition reactions (3) and (4). Table 2 reveals that in fact the trend is opposite to that expected from ΔH(MO−H). That is, the endothermicities of (3) and (4) increase from bottom to top of a TM triad and from left to right of a TM series. Obviously, the trend-setting term for the reaction enthalpies of the addition reaction given in (8) and (9) must be ΔH(M−CH_2OH) and ΔH(M−OCH_3), respectively. We shall now provide a further analysis of the M−CH_2OH and M−OCH_3 bonds, as well as the dependence of their strength on the identity of the metal center.

An analysis of our calculations reveals that the M−OCH_3 bond has a σ as well as π component, whereas the M−CH_2OH bond primarily is of σ character. The σ bond is due to the interaction between a singly occupied metal d-based antibonding orbital, the SOMO of the hydroxy−metal fragment (the 14a′ orbital in Figure 5), and a singly occupied oxygen or carbon p-based orbital. The π interaction results from the interaction of an occupied oxygen lone-pair orbital and an empty d_π component on the metal center.

The σ bond represents essentially a transfer of charge from the SOMO of the hydroxy−metal fragment to the lower lying singly occupied oxygen or carbon p-based orbital (Figure 7). The M−OCH_3 π bond constitutes, on the other hand, a synergetic back-donation of charge accumulated on oxygen in the σ interaction. Table 4 displays the compositions of the σ- and π-bonding orbitals. The density in the σ-bonding orbital is polarized away from the metal. The polarization decreases from top to bottom of the TM triad and from left to right in the TM series, as the SOMO of the hydroxy−metal fragment (the 14a′ orbital in Figure 5) becomes less antibonding and more stable (see previous section).

We have also decomposed the total M−OCH_3 and M−CH_2OH bond energies according to the ETS method (Table 5). In the first place, the M−OCH_3 bond is stronger than the M−CH_2OH linkage on account of its additional π component as well as its higher polarity (Figure 7 and Table 5). Further, a stronger M−OCH_3 bond energy correlates with a stronger polarization in the σ bond and a higher energy of the hydroxy−metal fragment SOMO. The relativistic destabilization[40] of d orbitals, and thus the SOMO, helps to further strengthen the M−OCH_3 and M−CH_2OH bonds, particularly for 5d TM's.

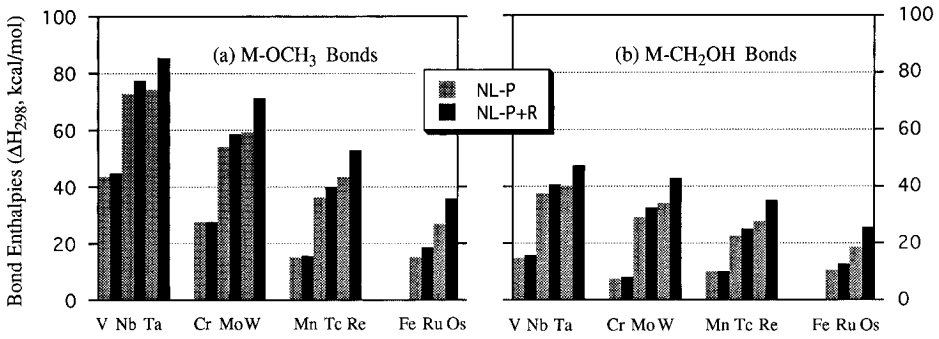

Figure 7. Plot of bond strengths for the M−OCH_3 and M−CH_2OH bonds of the O−H and C−H bond addition products.

Table 5. Bond Energy Decomposition Analyses for Cr, Mo, W, and Ru Systems[a]

bonds	M	E_{BD}	ΔE_{orbit}	ΔE_{steric}	ΔE_{prep}[b]
M−OCH_3	Cr	33	−130	73	21 + 3
	Mo	60	−147	71	14 + 2
	W	65	−143	63	13 + 2
	Ru	25	−105	63	18 + 2
M−CH_2OH	Cr	11	−94	54	24 + 5
	Mo	33	−117	59	20 + 5
	W	38	−119	57	19 + 5
	Ru	15	−91	52	21 + 3

[a] Electronic energies in kcal/mol. [b] The first term is due to the metal fragment, and the second term stems from the OCH_3 or CH_2OH moiety.

It is interesting to note how the energy for the SOMO of the hydroxy−metal fragment has an adverse influence on the endothermicities of, respectively, the abstraction and addition reactions. A high SOMO energy will weaken the MO−H bond and make the abstraction reaction highly endothermic. On the other hand, the same high SOMO energy makes the M−OCH_3 and M−CH_2OH bonds more polar and stronger which will result in low endothermicity for the addition reactions. Thus, the SOMO is ultimately responsible for the adverse trends in the abstraction and addition reaction enthalpies (Table 2).

Validation of the Perturbative Approach. It is by now well established that nonlocal corrections to the simple LDA theory play a crucial role in describing energetics correctly. In our studies of systems containing only main group elements,[17] we have demonstrated that the nonlocal corrections can be introduced efficiently in a perturbative approach based on LDA densities, NL-P. We shall now validate this approach for TM systems by comparing the NL-P energies presented here with estimates obtained from calculations in which nonlocal corrections have been taken into account in a self-consistent fashion, NL-SCF. Our comparison will involve processes 1−4 in the case of MCl_2O_2 (M = Cr, Mo, W) and RuO_4.

Table 6 compares the NL-SCF bond energies based on the fully nonlocal geometry optimization to the results calculated from the NL-P scheme as employed in this study. It follows from Table 6 that the rms deviation of the NL-P bond energies from the NL-SCF values is only 0.4 kcal/mol for the four representative TM systems. The discrepancies between the NL-P and NL-SCF results are less than 0.4 kcal/mol for 8 out of 12 different bonds under investigation, and the largest error due to the NL-P approximation is found to be only 1.0 kcal/mol in the case of the $(O)_3Ru-CH_2OH$ bond. The present study includes relativistic effects to first order, NL-P+FO. Li and Ziegler[41] have previously shown that the first-order approach affords nearly the same M-L bond energies as the more rigorous and costly NL-SCF+QR method, in which both nonlocal and quasi-relativistic (QR) corrections are included self-consistently.

4. Summary

We have reported a set of calculations on structural and thermodynamic data related to the O−H and C−H bond activation processes of methanol by the group 5 through group 8 transition metal oxo complexes. The transition metal oxo complexes considered included MO_nCl_{4-n} with $n = 1$ for M = V, Nb, Ta, $n = 2$ for M = Cr, Mo, W, $n = 3$ for M = Mn, Tc, Re, and $n = 4$ for M = Fe, Ru, Os. The O−H and C−H bond activation processes were considered to take place by hydrogen abstraction by MO_nCl_{4-n} to produce $MO_{n-1}Cl_{4-n}(OH)$ (eqs 1 and 2 of Scheme 1) or by σ-bond addition to generate respectively $MO_{n-1}Cl_{4-n}(OH)(OCH_3)$ and $MO_{n-1}Cl_{4-n}(OH)(CH_2OH)$ (eqs 3 and 4 of Scheme 1).

The hydrogen abstraction processes (1) and (2) are in general endothermic. Further, the stronger O−H bond is harder to activate by abstraction. The strength of the MO−H bond in $MO_{n-1}Cl_{4-n}(OH)$ completely determines how the reaction enthalpy for the hydrogen abstraction processes are influenced by the metal center. The weaker the MO−H bond, the more endothermic the abstraction reaction. It is found that the endothermicity decreases from bottom to top within a TM triad and from left to right within a TM series. This trend is ultimately determined by the radial extension of the metal d orbitals and the associated energy of the antibonding and metal-based SOMO in $MO_{n-1}Cl_{4-n}(OH)$. Thus, the more diffuse the d orbital, the higher the SOMO energy, the weaker the MO−H bond, and the higher the endothermicity of the abstraction processes (1) and (2).

The addition reactions (3) and (4) of Scheme 1 are more facile than the abstraction processes (1) and (2), with O−H addition being favored over C−H addition. The way in which the reaction enthalpies of (3) and (4) are influenced by the metal center is determined by, respectively, the M−OCH_3 and M−CH_2OH bond energies. The weaker the bonds, the more endothermic the addition reactions. It is found that the endothermicity increases from bottom to top within a TM triad and from

(41) (a) Li, J.; Schreckenbach, G.; Ziegler, T. *J. Am. Chem. Soc.* **1995**, *117*, 486. (b) Ziegler, T.; Li. J.; Schreckenbach, G. *Inorg. Chem.* **1995**, *34*, 3245. (c) Li, J.; Schreckenbach, G.; Ziegler, T. *J. Phys. Chem.* **1994**, *98*, 4838.

Table 6. Comparison of the Bond Energies[a] Calculated at the NL-P and NL-SCF Levels

	Cr		Mo		W		Ru	
	NL-P	NL-SCF	NL-P	NL-SCF	NL-P	NL-SCF	NL-P	NL-SCF
MO−H	66.5	66.9	50.1	50.5	47.4	47.6	71.4	71.7
M−OCH_3	33.1	33.3	59.8	59.9	65.1	64.9	22.0	22.0
M−CH_2OH	11.6	12.2	33.1	33.2	38.2	38.3	14.9	15.9

[a] Electronic energies, in kcal/mol.

left to right within a TM series. This trend is ultimately determined by the energy of the antibonding and metal-based SOMO in $MO_{n-1}Cl_{4-n}(OH)$ and by the radial extension of the metal d orbitals. Thus, the more diffuse the d orbital, the higher the SOMO energy, the stronger the M−OCH_3 and M−CH_2OH bonds, and the lower the endothermicity of the addition processes (3) and (4).

The periodic trends in the endothermicities of the abstraction reactions (1) and (2) are exactly opposite to those of the addition reactions (3) and (4), and the determining factors are for both reaction types the radial extension of the metal d orbital and the associated energy of the SOMO for the $MO_{n-1}Cl_{4-n}(OH)$ species.

Hydrogen abstraction from the O−H bond is not likely. However, hydrogen abstraction from the C−H bond might be possible with late transition metals of the first TM series. Addition is more facile than abstraction for all metals. For early transition metals, O−H addition is favored over C−H addition. However, O−H and C−H addition are both likely for late transition metals. These findings seem to be in agreement with experimental studies on the oxidation of ethers and alcohols by oxometal complexes.

The structures and vibrational frequencies for the $MO_{n-1}Cl_{4-n}$ species as determined by DFT at the LDA level are in better agreement with experiment than previous estimates based on HF *ab initio* theory.

Acknowledgment. This investigation was supported by the Natural Sciences and Engineering Research Council of Canada (NSERC) as well as the donors of the Petroleum Research Fund, administered by the American Chemical Society.

OM9600203